Contrib Mineral Petrol (1994) 116:239–246

Contributions to Mineralogy and Petrology

Hercynite as the product of staurolite decomposition in the contact aureole of Vedrette di Ries, eastern Alps, Italy

Bernardo Cesare

Dipartimento di Mineralogia e Petrologia, Università di Padova, I-35137 Padova, Italy

Received February 19, 1993 / Accepted November 5, 1993

Abstract. Metapelitic hornfelses in the contact aureole of the Vedrette di Ries pluton exhibit the terminal decomposition of Zn-poor Fe-staurolite in a muscovite-quartz-free domain. The reaction takes place only within coarse-grained sillimanite that has replaced andalusite porphyroblasts during prograde metamorphism. The product is a gahnite-poor hercynitic spinel, which occurs as very small grains closely associated in space with resorbed staurolite. Microstructural observations indicate that hercynite growth postdates the pseudomorphs of sillimanite after andalusite. The textural evidence for a genetic relationship between hercynite and staurolite is confirmed by the identical Fe/Mg/Zn ratios of the two minerals, which causes the collinearity of hercynite, staurolite and Al_2SiO_5 in FeO-MgO-ZnO-Al_2O_3-SiO_2-H_2O composition space (FMZASH), and indicates hercynite formed by the reaction:

Fe-staurolite = 3.85hercynite
+ 5.1sillimanite + 2.55quartz + $2H_2O$

Staurolite inclusions within andalusite did not break down to form hercynite, indicating a kinetic control, as well as little overstepping of the equilibrium conditions, of the reaction forming hercynite. Assuming overstepping did not occur, modelling of the reaction with existing thermodynamic data in the simplified FASH system suggests that the terminal breakdown of staurolite to form hercynite occurred at 2.5–3.75kbar and 585–655°C.

Introduction

Hercynite-rich, ternary Fe-Mg-Zn spinel is a typical mineral of both quartz-bearing (Waters 1991) and quartz-free metapelitic rocks (Ganguly 1972; Harris 1981) that form under low-pressure high-temperature conditions in the granulite facies (Stoddard 1979; Clarke and Powell 1991; Sengupta et al. 1991) or upper-amphibolite facies of regional (Harley and Fitzsimmons 1991) and contact metamorphism (Loomis 1972; Pattison and Tracy 1991 and references therein).

Several equilibria, based both on field evidence and experimental results, have been modelled to constrain the prograde appearance of hercynite. These commonly involve sillimanite and ferromagnesian reactant phases such as Fe-cordierite (Richardson 1968; Harris 1981), garnet (Shulters and Bohlen 1989; Harley and Fitzsimmons 1991) or Fe-staurolite (Richardson 1968; Ganguly 1972). In other instances, the appearance of gahnite-rich spinel has been attributed to the decomposition of either sphalerite (Spry and Scott 1986), or biotite (Montel et al. 1986), or, most frequently, to the breakdown of Zn-rich staurolite in assemblages both bearing (Schumacher 1985) and devoid of muscovite + quartz (Atkin 1978; Loomis 1972; Stoddard 1979: Tuccillo et al. 1992).

A genetic relationship between Zn-bearing staurolite and hercynite is predictable since Zn easily substitutes for Fe^{2+} in tetrahedral coordination, and this crystal-chemical configuration only occurs in staurolite and spinel among the minerals typical of high-grade metapelites. Evidence for the interrelationship between staurolite and hercynite, although rejected in some circumstances (Spry and Scott 1986), has been texturally documented by several authors, even during lower amphibolite-facies retrograde metamorphism, with the overgrowth of staurolite on gahnite-rich spinel (Moore and Reid 1989).

The reaction:

$$St \Leftrightarrow Her + Al_2SiO_5 + Qtz + H_2O \quad (1)$$

(mineral abbreviations according to Kretz 1983) has been proposed for explaining examples of either prograde hercynite (Loomis 1972; Tuccillo et al. 1992) or retrograde staurolite growth (Moore and Reid 1989). However in none of these cases was the stoichiometry of the reaction completely balanced because of the different Fe/Mg/Zn ratios of coexisting staurolite and spinel.

This contribution describes an example of hercynite growth through the breakdown of Zn-poor staurolite in metapelites from the contact aureole of the Vedrette di Ries pluton. On the basis of microstructural evidence and

because the Zn/Fe/Mg ratios of staurolite and hercynite are equal, reaction (1) is considered to have actually taken place in the muscovite + quartz-free domains of the rock.

Geo-petrographic setting

The staurolite-hercynite assemblage is found in the pelitic hornfelses located at the northern intrusive contact of the Oligocene (Borsi et al. 1979) tonalitic pluton of Vedrette di Ries (eastern Italian Alps, Fig. 1). These rocks are part of the Austroalpine crystalline basement, which displays a polymetamorphic history of pre-Alpine and Alpine age (Borsi et al. 1973, 1978; Frank et al. 1987), that culminated with a contact metamorphic event in the aureole of the tonalite.

The reaction sequence developed during the contact metamorphism can be ascribed to type 2bii in the facies series scheme proposed by Pattison and Tracy (1991). Typical parageneses developed in the inner contact aureole contain biotite, garnet, fibrolitic and coarse-grained sillimanite, muscovite, quartz, oligoclase, ilmenite and graphite; metastable relicts of andalusite are also common. Staurolite is generally absent in the highest grade Al-rich metapelites of the aureole, due to its complete breakdown in the presence of quartz and muscovite (Cesare 1992). However, staurolite may be preserved locally where it is completely armoured within andalusite relicts. The "second sillimanite" assemblage (Evans and Guidotti 1966) is sporadically developed but not exceeded, as the association of muscovite plus quartz is stable up to the intrusive contact. Maximum temperatures at the pluton-country rock interface have been estimated to be in the range 600–620°C; the contact metamorphism is considered isobaric at a minimum pressure of 2.9 kbar (Cesare 1992).

Hercynite has been found in a few samples from the uppermost grade zones of the aureole, within one hundred metres of the tonalite; in these rocks prismatic sillimanite directly replaces andalusite, by the paramorphic mechanism described by Kerrick and Woodsworth (1989) and Vernon (1987). The rock matrix adjacent to the pseudomorphs contains quartz, biotite, sillimanite, muscovite, ilmenite and graphite. Neither garnet nor cordierite occur in the Her-bearing samples.

Figure 2 shows the And ⇒ Sil replacement and the marked contrast in the amount of inclusions within the two minerals: sillimanite generally contains very few inclusions of staurolite in comparison to adjacent andalusite. Tiny grains (< 30 μm) of hercynitic green spinel occur only within the pseudomorphs of coarse sillimanite after andalusite (Fig. 3), and have not been observed in andalusite or in the rock matrix. The textural occurrence of hercynite differs from the sillimanite-spinel segregations described by Stoddard (1979), that did not form after andalusite.

Because of the extremely fine grain size of the crystals, the relationships between staurolite and hercynite have been investigated by scanning electron microscopy (Fig. 4). Three phases can be detected as inclusions in sillimanite: staurolite, hercynite and ilmenite. Staurolite generally displays an anhedral shape within sillimanite, whereas it is idioblastic where included in andalusite; hercynite occurs as rounded crystals, which appear to be chemically homogeneous under BSE (back-scattered electron) analysis. Intergrowth or overgrowth textures cannot be observed among staurolite and hercynite. Ilmenite appears to be equally distributed within the pseudomorph sites, suggesting that it had a refractory behaviour with respect to the transition of andalusite to sillimanite.

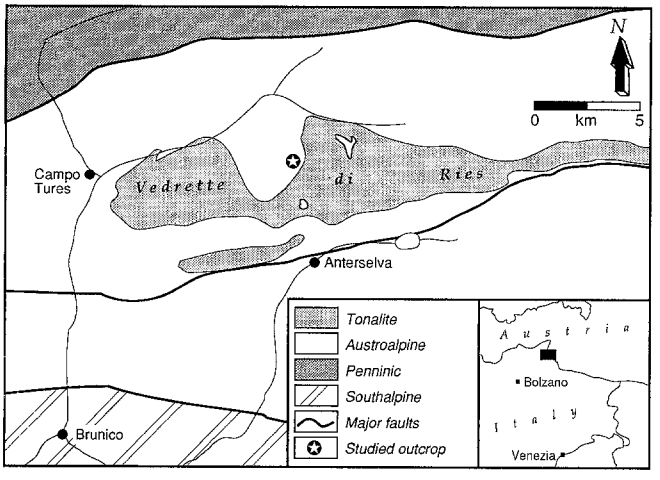

Fig. 1. Simplified geologic map of Vedrette di Ries pluton and neighbouring crystalline basement units

Chemical composition of co-existing hercynite and staurolite

Chemical analyses of spinel and staurolite were obtained using a CAMECA SX50 electron microprobe. Spinel and

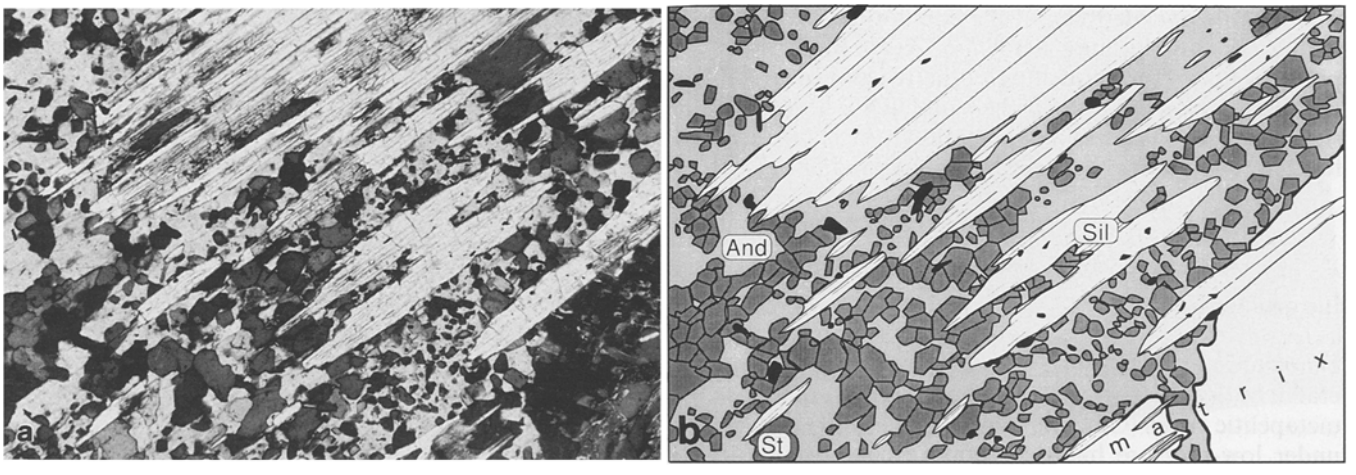

Fig. 2. Photomicrograph (**a**) and identifying sketch at the same scale (**b**) showing paramorphic replacement of andalusite by prismatic sillimanite. Andalusite contains abundant inclusions of staurolite; sillimanite is almost inclusion free. Small black grains are ilmenite. Crossed polars, base of photograph 1.6 mm

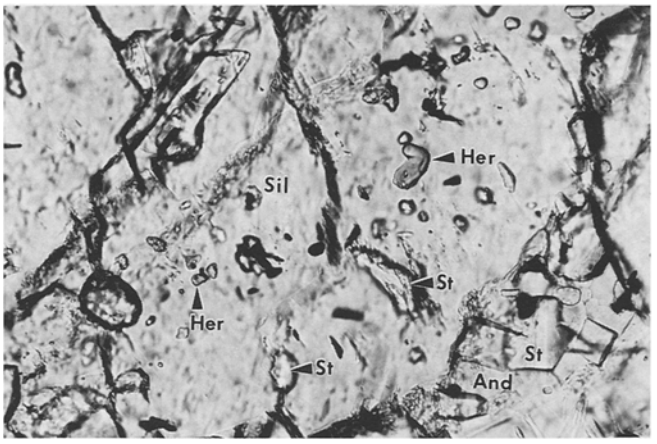

Fig. 3. Sillimanite crystals replacing andalusite, in a section at a high angle to sillimanite c-axis. Anhedral staurolite, *St*, small hercynite crystals, *Her*, and ilmenite are included in sillimanite, *Sil*. Adjacent andalusite, *And*, contains perfectly euhedral staurolite. Plane-polarized light, base of photograph 0.33 mm

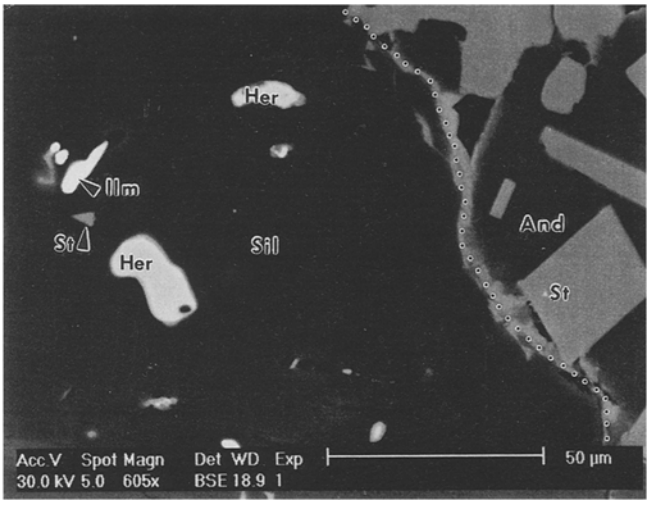

Fig. 4. Backscattered-electron (BSE) image of an area of Fig. 3. Highly reflecting minerals in dark Al_2SiO_5 matrix (both sillimanite, *Sil*, and andalusite, *And*, possibly quartz) are hercynite, *Her*, and ilmenite, *Ilm*. Staurolite, *St*, (less bright) occurs in two contrasting shapes: small and anhedral within sillimanite, coarser and euhedral in andalusite. *Dotted line* marks And-Sil grain boundary. Hercynite only occurs *within* sillimanite

Table 1. Chemical composition of staurolite, hercynite and Al_2SiO_5 polymorphs within And-Sil pseudomorph site of Fig. 3. See text for normalizing procedures and assumptions

	Staurolite					Hercynite					Sillimanite		Andalusite		
	1	2	3	4		5	6	7	8		9	10	11	12	13
SiO_2	26.65	26.74	27.46	27.15	SiO_2	0.06	0.02	0.03	0.07	SiO_2	35.85	36.00	37.06	36.85	36.93
TiO_2	0.51	0.46	0.40	0.46	TiO_2	0.01	0.02	0.00	0.00	Al_2O_3	62.69	63.08	62.56	63.22	61.46
Al_2O_3	55.16	55.54	55.41	54.06	Al_2O_3	58.88	58.44	58.49	58.66	Fe_2O_3	0.80	0.41	0.37	0.25	1.06
FeO	11.97	12.52	12.34	12.74	FeO	33.37	33.17	33.15	33.31	MnO	0.00	0.03	0.03	0.00	0.01
MnO	0.56	0.58	0.52	0.54	MnO	0.65	0.59	0.61	0.58	MgO	0.04	0.02	0.11	0.03	0.34
MgO	1.20	1.13	1.15	1.31	MgO	3.42	3.44	3.49	3.48						
ZnO	0.83	0.90	0.85	0.84	ZnO	3.09	2.81	2.92	3.08						
H_2O	2.14	2.16	2.17	2.14											
Total	99.02	100.03	100.32	99.24	Total	99.48	98.49	98.69	98.98	Total	99.38	99.54	100.13	100.35	99.80
Si	7.451	7.420	7.582	7.601	Si	0.002	0.001	0.001	0.002	Si	0.977	0.978	0.999	0.991	1.001
Ti	0.107	0.097	0.083	0.097	Ti	0.000	0.000	0.000	0.000	Al	2.012	2.020	1.987	2.004	1.963
Al	18.180	18.164	18.031	17.839	Al	1.982	1.985	1.983	1.983	Fe^{3+}	0.016	0.009	0.008	0.005	0.022
Fe^{2+}	2.800	2.906	2.849	2.983	Fe^{2+}	0.797	0.799	0.797	0.794	Mn	0.000	0.001	0.001	0.000	0.000
Mn	0.132	0.137	0.123	0.128	Mn	0.016	0.014	0.015	0.014	Mg	0.002	0.001	0.004	0.001	0.014
Mg	0.498	0.466	0.473	0.547	Mg	0.146	0.148	0.149	0.149						
Zn	0.171	0.185	0.173	0.174	Zn	0.065	0.060	0.062	0.065						
OH	4.000	4.000	4.000	4.000											
X_{Fe}	0.849	0.862	0.858	0.845	X_{Fe}	0.846	0.844	0.842	0.842						
X_{Zn}	0.049	0.052	0.050	0.047	X_{Zn}	0.065	0.059	0.062	0.065						
$X_{Fe'}$	0.844	0.858	0.854	0.841											
$X_{Zn'}$	0.051	0.054	0.051	0.048											

Analyses 1–3, staurolite inclusions in sillimanite; 4, staurolite within andalusite; 5–8, hercynite; 9, 10, prismatic sillimanite; 11, 12, andalusite; 13, pink pleochroic andalusite core, enriched in iron. $X_{Fe} = Fe/(Fe+Mg)$; $X_{Zn} = Zn/(Zn+Fe+Mg)$; $X_{Fe'}$ and $X_{Zn'}$ values recast assuming Fe = Fe − Ti to account for Ti in staurolite and the production of ilmenite during reaction (4′)

staurolite formulas in Table 1 were calculated on the basis of 4 and 48 oxygens, respectively. Because staurolite occurs in association with graphite and ilmenite, it was assumed to contain negligible amounts of ferric iron (see Dyar et al. 1991; Holdaway et al. 1991). Table 1 also reports the chemical composition of andalusite and sillimanite, calculated on the basis of 5 oxygens and only ferric iron.

Due to the difficulty of analysing the very fine grained spinel, all compositions were measured in the cores of the

grains; consequently chemical zoning could not be evaluated. Spinel analyses from different grains are very similar: the composition is essentially that of a ternary Fe-Mg-Zn hercynite, with galaxite ($MnAl_2O_3$) component less than 1.6 mol%. The Zn content is low, around 0.06–0.07 cations per formula unit, and is similarly low in staurolite (less than 1.0 wt% ZnO).

Staurolite within coarse sillimanite is iron rich [Fe/(Fe+Mg) = 0.85] and shows no compositional zoning. Although most of the staurolite evidently reacted during the alteration of andalusite to sillimanite (cf. Fig. 2), the staurolite remnants within sillimanite have the same Fe/(Fe+Mg) and zinc concentration as the crystals included in andalusite. Cation stoichiometries formulated on the basis of 48 oxygens, 4 hydroxyls and ferrous iron are comparable to those of Fe^{3+}-poor staurolite given by Holdaway et al. (1991), and closely match (particularly staurolite in andalusite, analysis 4) the charge balanced iron end-member formula $H_4Fe_{3.85}Al_{17.9}Si_{7.65}O_{48}$ of Holdaway et al. (1991). This formula will be used in the calculations below.

The Al_2SiO_5 polymorphs have low and similar Fe_2O_3 content; only the pink pleochroic cores of andalusite show a slight enrichment in Fe^{3+} (analysis 13).

Modelling of the staurolite-out reaction

Textural constraints

The textural observations that suggest a genetic relationship between staurolite and hercynite are:

1. Staurolite is the only ferromagnesian silicate which occurs within sillimanite crystals.
2. Staurolite within prismatic sillimanite is very scarce in comparison to staurolite within adjacent andalusite porphyroblasts (Fig. 2).
3. Staurolite included in sillimanite exhibits resorbed grain boundaries, whereas it is euhedral when included in andalusite (Fig. 4).
4. Hercynite only occurs in close association with staurolite as inclusions *within* the coarse-grained prismatic sillimanite which forms pseudomorphs after andalusite (Fig. 3). Hercynite does not occur at the And-Sil grain boudaries (Fig. 4).

Based on the above evidence it may be inferred that during heating the staurolite inclusions in andalusite underwent two sequential dissolution events, in two distinct microstructural domains. The first event, which is accompanied by the disappearance of most staurolite, is coeval with the replacement of andalusite by sillimanite (Fig. 2). The replacement may have caused staurolite, formerly armoured by andalusite, to interact with the Ms + Qtz-bearing matrix by means of an intergranular fluid phase, and allow the breakdown of staurolite in the presence of muscovite and quartz to take place by reactions such as

$$St + Ms + Qtz = Bt + Sil + H_2O \quad (2)$$

or

$$St + Ms + Qtz = Grt + Bt + Sil + H_2O. \quad (3)$$

Because biotite occurs in the rock matrix of the sample examined, whereas garnet is absent, overstepped reaction (2) is considered the most likely to have determined staurolite decomposition during the And ⇒ Sil replacement. This stage was not accompanied by the growth of hercynite, as hercynite does not occur at the And-Sil grain boundaries.

The second decomposition episode occurred within coarse sillimanite. Inasmuch as tiny staurolite crystals are also present within the sillimanite, they probably represent relicts that did not react completely and/or remained isolated from the adjacent matrix. Thus, they effectively comprised a Qtz-Ms-absent local system in which reaction (2) could not occur and staurolite persisted stably up to its terminal breakdown. The occurrence of hercynite exclusively as inclusions within sillimanite, as well as the resorbed shape of adjacent staurolite, suggest hercynite is the product of the terminal decomposition of staurolite, which postdates the And ⇒ Sil replacement. The following discussion will only deal with this latter episode of staurolite breakdown.

Compositional constraints

Consider the chemical system defined by sillimanite and its inclusions of staurolite, hercynite and ilmenite. If it is assumed that titanium is only present in ilmenite (cf. Table 1), TiO_2 can be treated as an "inert" component, ilmenite can be ignored, and the remaining three phases described in terms of the six oxides: FeO, MgO, ZnO, Al_2O_3, SiO_2 and H_2O ("FMZASH" system).

The chemical relationships between hercynite and staurolite are evaluated by projecting the relative amounts of their tetrahedrally coordinated divalent cations (Fe, Mg, Zn), as in Fig. 5. Projected compositions of both minerals overlap in a very narrow field, indicating that staurolite and hercynite have nearly identical Fe/Mg/Zn ratios: $Fe_{0.80\pm0.01}Mg_{0.145\pm0.01}Zn_{0.055\pm0.01}$. Be-

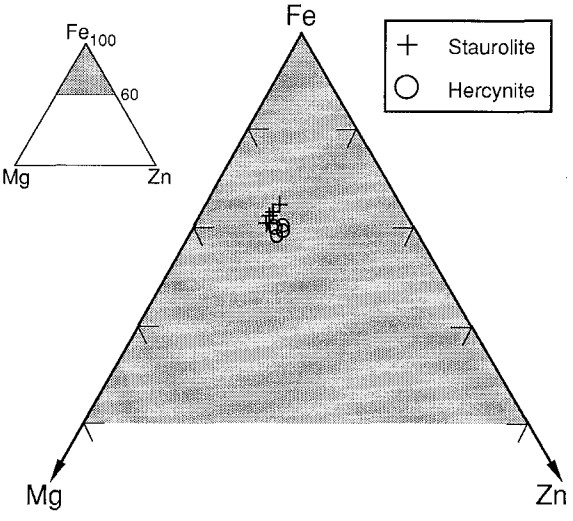

Fig. 5. Fe-Mg-Zn plot of staurolite, *crosses*, and hercynite, *circles*. Mineral compositions nearly overlap within a narrow compositional field of $Fe_{0.80\pm0.01}Mg_{0.145\pm0.01}Zn_{0.055\pm0.01}$

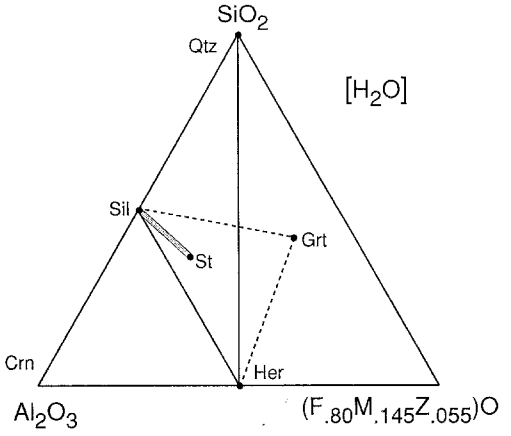

Fig. 6. Ternary SiO_2-Al_2O_3-(FMZ)O projection through H_2O of degenerate FMZASH system. *Shaded line* represents a possible range of bulk composition determined by staurolite inclusions in sillimanite. The breakdown of staurolite stabilizes the three phase field Qtz-Sil-Her. Although garnet and cordierite could not be projected in this chemography, as they do not partition Zn, *dashed lines* schematically illustrate the assemblage that would result from reaction (7). Mass-balance constraints hamper such configuration (see discussion section)

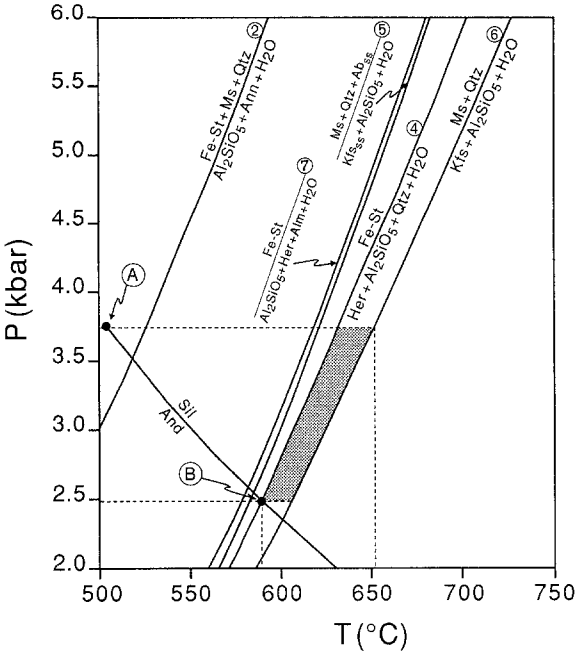

Fig. 7. Simplified petrogenetic grid with calculated FASH, KFASH and KNASH equilibria relevant to staurolite dehydration, assuming a C-O-H, H:O = 2, graphite-saturated fluid (Connolly and Cesare 1993). And-Sil transition from Holdaway and Mukhopadhyay (1993); *A*, Ky-And-Sil invariant point; *B*, And-Sil-Her-St-Qtz-H_2O invariant point. Numbers of equilibrium curves as in text; *ss subscript* indicates K-Na solid solution. *Shaded area* indicates the inferred metamorphic *P-T* field of equilibration for hercynite-bearing rocks in the Vedrette di Ries aureole

cause of the very similar Fe/Mg/Zn ratios of staurolite and hercynite, a near collinearity exists among the above minerals and sillimanite in FMZASH compositional space. This collinearity results in a degeneracy within the six component system, such that the coexisting phases can be described in terms of only four components: $(Fe_{0.80}Mg_{0.145}Zn_{0.055})O$-$Al_2O_3$-$SiO_2$-$H_2O$, and represented by the triangular chemography $(Fe_{0.80}Mg_{0.145}Zn_{0.055})O$-$Al_2O_3$-$SiO_2$, projected through H_2O, of Fig. 6. This choice of components is valid because other ferromagnesian phases like garnet or cordierite, which would not partition Zn and could have different Fe/(Fe + Mg) values, are not present in the rock.

In Fig. 6 the bulk composition of the system lies along the St-Sil join, on the corundum-undersaturated side of the Sil-Her tie-line. Given that both garnet and cordierite are absent, it follows that the most likely reaction for the breakdown of staurolite can be identified as St ⇒ Her + Sil + Qtz, and balanced (using staurolite formula $H_4Fe_{3.85}Al_{17.9}Si_{7.65}O_{48}$) as:

$$\text{Fe-St} \Leftrightarrow 3.85\text{Her} + 5.1\text{Sil} + 2.55\text{Qtz} + 2H_2O. \quad (4)$$

Combining the chemical relationships and the textural evidence, and given that three of the four solid phases involved in the dehydration reaction are found in close association, reaction (4) is a plausible model for the growth of hercynite in the contact aureole of Vedrette di Ries pluton.

Pressure-temperature conditions

The *P-T* conditions at which the crystallization of hercynite takes place by reaction (4) can be evaluated in a semi-quantitative way by calculating the equilibrium curves of staurolite breakdown in the simplified FASH and KFASH systems. This simplification has been used because of the poor knowledge of the thermodynamic properties of Mg-Zn end-members for staurolite. The calculations shown in Fig. 7 have been done using the approach of Connolly (1990) and an updated version of the thermodynamic dataset of Berman (1988). Since graphite occurs in the rock and ilmenite is the only opaque phase present, the fluid was assumed to be a C-O-H mixture, with a 2:1 atomic H:O ratio (Connolly and Cesare 1993).

The consistency of the relative position of the calculated equilibrium curves in *P-T* space can be checked easily against the reaction sequence deduced by the field observations. In the thermodynamic calculation of Fig. 7, the FASH hercynite-forming reaction (4) is predicted to occur at temperatures lower than (or overlapping, depending on the amount of paragonite component in muscovite) the first appearance of alkali feldspar, bounded by the reactions

$$Ms + Qtz + Ab_{ss} = Kfs_{ss} + Al_2SiO_5 + H_2O \quad (5)$$

and

$$Ms + Qtz = Kfs + Al_2SiO_5 + H_2O. \quad (6)$$

This calculated sequence is the same as that recorded by the hornfelses close to the intrusive body (Cesare 1992), and is also in agreement with other petrogenetic grids for metapelitic rocks (Yardley 1981; Spear and Cheney 1989). In fact the matrix of the sample where her-

cynite has formed contains muscovite plus quartz but not K-feldspar.

The maximum isobaric temperature difference between the equilibrium curves for reaction (4) and (6) is on the order of 20°C. This difference, although resulting from calculations in the simplified FASH system, is considered to be reliable because the "second sillimanite" assemblage actually develops in the hornfelses a few metres closer to the contact.

Assuming that no significant overstepping of the equilibrium conditions occurred during reaction (4) (see discussion below), the range of pressure and temperature at which the rock equilibrated can be tightly constrained via a "bathogradic" approach (Carmichael 1978), since metamorphism followed an isobaric heating path starting in the andalusite field, and reaction (4) took place in the sillimanite stability field. The *P-T* conditions of equilibration are constrained by: (1) equilibrium (4) at low temperature (hercynite growth); (2) equilibrium (7) at high temperature (persistence of the assemblage muscovite + quartz); (3) the isobaric line intersecting the Al_2SiO_5 triple point (A in Fig. 7) at high pressure (maximum stability of andalusite); (4) the isobar intersecting the And-Sil-St-Her-Qtz-H_2O invariant point (B in Fig. 7) at low pressure (hercynite growth within the stability field of sillimanite).

The absolute values of the *P-T* extremes are dependent on the location of the And-Sil equilibrium curve. In this study the curve of Holdaway and Mukhopadhyay (1993) has been adopted, assuming that it has not been displaced by partitioning of minor elements between andalusite and sillimanite (Grambling and Williams 1985; Kerrick and Speer 1988): in fact co-existing andalusite and sillimanite have equal Fe^{3+} concentrations. It follows that the metamorphic conditions of hercynite formation via reaction (4) are bracketed between 585°C and 655°C and between 2.5 and 3.75 kbar.

Discussion

Equations (1) and (4) correspond to the reaction previously proposed in both prograde and retrograde scenarios by Loomis (1972), Moore and Reid (1989) and Tuccillo et al. (1992), with slightly different stoichiometric coefficients because of the staurolite formula adopted. However, since Zn is present in the system, reaction St ⇔ Her + Al_2SiO_5 + Qtz + H_2O requires collinearity between Al_2SiO_5, hercynite and staurolite in FMZASH composition space, and such constraint was not obeyed in those cases. Thus, either the presence of an additional ferromagnesian or zincian phase was necessary to maintain mass-balance, or the system was considered open to one component during the reaction (e.g. Fe, Moore and Reid 1989). In contrast, the chemical collinearity in FMZASH system shown in this study permits the stoichiometry of reaction (4) to be respected. Even if the small amount of titanium in staurolite is taken into account, it can readily be accommodated by the production of 0.01 moles ilmenite per mole of staurolite (see Table 1). This would imply the subtraction of 0.005 moles hercynite and the addition of 0.0025 moles sillimanite from the stoichiometric coefficients of reaction (4), to give:

$$St \Leftrightarrow 3.845Her + 5.1025Sil + 2.55Qtz + 2H_2O + 0.01Ilm \quad (4')$$

The addition of titanium to the system does not change substantially the proposed reaction (4), because it does not affect the Fe/Mg/Zn relationships between staurolite and hercynite. The subtraction of ilmenite component from staurolite, in fact, makes the values of Fe/Mg/Zn ratios of staurolite and hercynite even closer to each other (see recalculated $X_{Fe'}$ and $X_{Zn'}$ parameters in Table 1), and results in a nearer approach to collinearity between Sil, Her and St.

Theoretically, the preferential partitioning of zinc into hercynite and staurolite and among them (hercynite being Zn-richer than staurolite, Stoddard 1979; Moore and Reid 1989), should cause the univariant FASH equilibrium (4) to become trivariant in the FMZASH system. However, in the present case equilibrium (4) seems to remain univariant even in the presence of Mg and Zn in the rock, as testified by the nearly identical Fe/Mg/Zn ratios. An explanation for this behaviour is that staurolite may exhibit azeotropic phase relations with spinel in the FMZASH system and that the azeotropic composition of the minerals lies very close to $Fe_{0.80}Mg_{0.145}Zn_{0.055}$. Only at the azeotropic composition the Fe/Mg/Zn ratio values coincide, decreasing the degrees of freedom of the equilibrium; for any other composition there is generally a different partitioning of the divalent cations between the phases.

According to Fig. 7 reaction (4) would be metastable in the FASH system with respect to reaction

$$Fe\text{-}St \Leftrightarrow Sil + Her + Alm + H_2O \quad (7)$$

that would occur at temperatures 10–20°C below the FASH equilibrium of (4). The occurrence of reaction (7), schematically represented by the dashed lines in Fig. 6, is considered unlikely for two reasons: the mass-balance prediction for staurolite, hercynite and garnet to have different Fe/Mg/Zn ratios and/or to be zoned, and the lack of garnet in the rock. Two explanations for this apparent inconsistency are that equilibrium (7) was overstepped because of the sluggish kinetics of garnet nucleation and the rapid heating rate of contact metamorphism, or that the reaction sequence is actually reversed in the full FMZASH system.

A kinetic control on the reaction mechanisms is also evident in that hercynite growth appears to be controlled by the site where staurolite occurs. In fact, although reaction (4) could have just as well taken place in the staurolite-rich, adjacent andalusite, it only developed within sillimanite. The presence of closely spaced microdomains of local equilibrium suggests that the breakdown of staurolite was inhibited by the absence of pre-existing nuclei of the stable Al_2SiO_5 polymorph, sillimanite. Thus, it may be deduced that not only was the enclosure by Al_2SiO_5 necessary to keep staurolite isolated from the Qtz-Ms-bearing matrix and allow it to persist to higher temperatures, but also that a specific type of aluminum silicate (i.e. sillimanite) was necessary to permit reaction (4). The

contrasting behaviour among staurolite inclusions in adjacent Al_2SiO_5 crystals indicates that the reaction mechanisms for the decomposition of staurolite armoured in andalusite were too slow, probably because of difficulties in the nucleation of new sillimanite grains, and suggests that equilibrium conditions for reaction (4) should have been only slightly exceeded during the growth of hercynite within sillimanite. Given such absence of significant overstepping, it can be concluded that the *P-T* values determined in Fig. 7 approach quite closely the actual conditions during the contact metamorphism.

Finally, the problem of the absence of quartz within the reaction site is discussed. Reaction (4) requires that quartz also be produced by staurolite decomposition. The mode of quartz produced by this reaction is on the order of one third that of hercynite; this quantity should be detectable by X-ray mapping, but SEM analysis did not give positive results. Quartz could be present within sillimanite, but not detected either because of the very small area available for SEM investigation, or because of its very fine grain size. In either case, only a transmission electron microscopy study could give a definitive answer to the problem. A third explanation is that silica produced by reaction (4) was transported away from the reaction site with the H_2O released by staurolite dehydration, and was precipitated in the adjacent Qtz-bearing matrix. Although the presence of quartz within sillimanite would make the argument more straightforward, the chemical and microstructural constraints discussed here are considered strong enough to support reaction (4) as the model for hercynite formation during the breakdown of Zn-poor staurolite.

Acknowledgements. I would like to thank J. Connolly, A. Della Giusta, C. Guidotti, M. Holdaway, L. Hollister, F.P. Sassi and an anonymous reviewer for their helpful comments and improvements of the manuscript, as well as V. Trommsdorff for encouraging me to work on the St-Her relationships. The IMP-ETH, Zürich kindly provided microprobe facilities for this research, while P. Guerriero (ICTR, CNR Padova) assisted during SEM work. Grants from Italian MURST 40% (FPS) are gratefully acknowledged.

References

Atkin BP (1978) Hercynite as a breakdown product of staurolite from within the aureole of the Ardara pluton, Co. Donegal, Eire. Mineral Mag 42:237–240

Berman RG (1988) Internally consistent thermodynamic data set for minerals in the system Na_2O-K_2O-CaO-MgO-FeO-Fe_2O_3-Al_2O_3-SiO_2-TiO_2-H_2O-CO_2. J Petrol 29:445–522

Borsi S, Del Moro A, Sassi FP, Zirpoli G (1973) Metamorphic evolution of the Austridic rocks to the south of the Tauern Window (eastern Alps). Radiometric and geo-petrologic data. Mem Soc Geol Ital 12:549–571

Borsi S, Del Moro A, Sassi FP, Zanferrari A, Zirpoli G (1978) New petrologic and radiometric data on the Alpine history of the Austridic continental margin south of the Tauern Window (eastern Alps). Mem Sci Geol 32

Borsi S, Del Moro FP, Sassi FP, Zirpoli G (1979) On the age of the Vedrette di Ries (Rieserferner) massif and its geodynamic significance. Geol Rundsch 68:41–60

Carmichael DM (1978) Metamorphic bathozones and bathograds: a measure of the depth of post-metamorphic uplift and erosion on the regional scale. Am J Sci 278:769–797

Cesare B (1992) Metamorfismo di contatto di rocce pelitiche nell'aureola di Vedrette di Ries (Alpi orientali - Italia) (unpublished). PhD Thesis, Univ Padova

Clarke GL, Powell R (1991) Proterozoic granulite facies metamorphism in the southeastern Reynolds Range, central Australia: geological context, *P-T* path and overprinting relationships. J Metamorphic Geol 9:267–282.

Connolly JAD (1990) Multivariable phase diagrams: an algorithm based on generalized thermodynamics. Am J Sci 290:666–718

Connolly JAD, Cesare B (1993) C-O-H-S fluid composition and oxygen fugacity in graphitic metapelites. J Metamorphic Geol 11:379–388

Dyar MD, Perry CL, Rebbert CR, Dutrow BL, Holdaway MJ, Lang HM (1991) Mössbauer spectroscopy of synthetic and naturally occurring staurolites. Am Mineral 76:27–41

Evans BW, Guidotti CV (1966) The sillimanite-potash feldspar isograd in western Maine, USA. Contrib Mineral Petrol 12:25–62

Frank W, Kralik M, Scharbert S, Thöni M (1987) Geochronological data from the eastern Alps. In: Flügel HW, Faupl P (Eds) Geodynamics of the eastern Alps, pp 272–281

Ganguly J (1972) Staurolite stability and related parageneses. Theory, experiments and applications. J Petrol 13:335–365

Grambling JA, Williams ML (1985) The effects of Fe^{3+} and Mn^{3+} on aluminum silicate phase relations in north-central New Mexico, U.S.A. J Petrol 26:324–354

Harley SL, Fitzsimmons ICW (1991) Pressure-temperature evolution of metapelitic granulites in a polymetamorphic terrane: the Rauer group, east Anctartica. J Metamorphic Geol 9:231–244

Harris N (1981) The application of spinel-bearing metapelites to *P/T* determinations: an example from south India. Contrib Mineral Petrol 76:229–233

Holdaway MJ, Mukhopadhyay B (1993) A reevaluation of the stability relations of andalusite: thermochemical data and phase diagram for the aluminum silicates. Am Mineral 78:298–315

Holdaway MJ, Mukhopadhyay B, Dyar MD, Dutrow BL, Rumble D, Grambling JA (1991) A new perspective on staurolite crystal chemistry: use of stoichiometric and chemical end-members for a mole fraction model. Am Mineral 76:1910–1919

Kerrick DM, Speer JA (1988) The role of minor element solid solution on the andalusite-sillimanite equilibrium in metapelites and peraluminous granitoids. Am J Sci 288:152–192

Kerrick DM, Woodsworth GJ (1989) Aluminum silicates in the Mount Raileigh pendant, British Columbia. J Metamorphic Geol 7:547–563

Kretz R (1983) Symbols for rock-forming minerals. Am Mineral 68:277–279

Loomis TP (1972) Contact metamorphism of pelitic rock by the Ronda ultramafic intrusion, southern Spain. Geol Soc Am Bull 83:2449–2474

Montel J, Weber C, Pichavant M (1986) Biotite-sillimanite-spinel assemblages in high-grade metamorphic rocks: occurrences, chemographic analysis and thermobarometric interest. Bull Mineral 109:555–573

Moore JM, Reid AM (1989) A Pan-African zincian staurolite imprint on Namaqua quartz-gahnite-sillimanite assemblages. Mineral Mag 53:63–70

Pattison DRM, Tracy RJ (1991) Phase equilibria and thermobarometry of metapelites. In: Kerrick DM (ed) Contact metamorphism. (Reviews in mineralogy 26) Mineral Soc Am, Washington, DC, pp 105–206

Richardson SW (1968) Staurolite stability in a part of the system Fe-Al-Si-O-H. J Petrol 9:467–88

Schumacher R (1985) Zincian staurolite in Glenn Doll, Scotland. Mineral Mag 49:561–571

Shulters JC, Bohlen SR (1989) The stability of hercynite and hercynite-gahnite spinels in corundum- or quartz-bearing assemblages. J Petrol 30:1017–1031

Sengupta B, Karmakar S, Dasgupta S, Fukuoka M (1991) Petrology of spinel granulites from Araku, Eastern Ghats, India, and a petrogenetic grid for sapphirine-free rocks in the system FMAS. J Metamorphic Geol 9:451–460

Spear FS, Cheney JT (1989) A petrogenetic grid for pelitic schists in the system SiO_2-Al_2O_3-FeO-MgO-K_2O-H_2O. Contrib Mineral Petrol 101:149–164

Spry PG, Scott SD (1986) Zincian spinel and staurolite as guides to ore in the Appalachians and Scandinavian Caledonides. Can Mineral 24:147–163

Stoddard EF (1979) Zinc-rich hercynite in high-grade metamorphic rocks: a product of the dehydration of staurolite. Am Mineral 64:736–741

Tuccillo ME, Metzger K, Essene EJ, Van Der Pluijm BA (1992) Thermobarometry, geochronology and the interpretation of *P-T-t* data in the Britt Domain, Ontario Grenville Orogen, Canada. J Petrol 33:1225–1259

Vernon RH (1987) Oriented growth of sillimanite in andalusite, Placitas-Juan Tabo area, New Mexico, U.S.A. Can J Earth Sci 24:580–590

Waters DJ (1991) Hercynite-quartz granulites: phase relations, and implications for crustal processes. Eur J Mineral 3:367–387

Yardley BWD (1981) A note on the composition and stability of Fe-staurolite. Neues Jahrb Mineral Monatsh 3:127–132

Editorial responsibility: V. Trommsdorff